A Histidine/Tryptophan π-Stacking Interaction Stabilizes the Heme-Independent Folding Core of Microsomal Apocytochrome b_5 Relative to that of Mitochondrial Apocytochrome b_5[†,‡]

Lijun Wang,[§] Na Sun,[§] Simon Terzyan,[#] Xuejun Zhang,[#] and David R. Benson*[,§]

Department of Chemistry, University of Kansas, Lawrence, Kansas 66045 and Crystallography Program, Oklahoma Medical Research Foundation, 825 NE 13th Street, Oklahoma City, Oklahoma 73104

Received August 2, 2006; Revised Manuscript Received September 1, 2006

ABSTRACT: The outer mitochondrial membrane isoform of mammalian cytochrome b_5 (OM b_5) is considerably more stable than its microsomal counterpart (Mc b_5), whereas the corresponding apoproteins (OM and Mc apo-b_5) exhibit similar stability. OM and Mc apo-b_5 are also similar in that their empty heme-binding pockets (core 1) are highly disordered but that the remainder of each apoprotein (core 2) displays substantial hololike structure. Core 1 residue 71 is leucine in all known mammalian OM b_5's and serine in the corresponding Mc proteins. Replacing Leu-71 in rat OM (rOM) b_5 with Ser has been shown to (1) decrease apoprotein thermodynamic stability by >2 kcal/mol and (2) extend conformational disorder beyond core 1 and into core 2, as evidenced in part by loss of a near-UV circular dichroism signal associated with the side chain of invariant residue Trp-22. Herein we report identification of a conserved Mc b_5 core 2 packing motif that plays a key role in stabilizing apoprotein conformation in the vicinity of Trp-22, thereby compensating for the presence of Ser at position 71: a π-stacking interaction between the side chains of Trp-22 and His-15 that is extended by hydrogen bonding between the side chains of His-15, Ser-20, and Glu-11. The corresponding conserved packing motif in OM b_5's differs in having arginine at position 15 and glutamate at position 20. We also present evidence indicating that the conserved Mc b_5 packing motif noted above contributes to the unusually extensive secondary structure exhibited by bovine Mc apo-b_5 in the urea-denatured state.

Mammals harbor two cytochrome b_5 genes (*1*), which likely arose via duplication of a primordial gene and subsequent functional divergence (*2*). One gene codes for a b_5 isoform that is targeted to the endoplasmic reticulum (microsomal, or Mc b_5),[1] the other for an isoform that is targeted to the outer mitochondrial membrane (OM b_5) (*3*). Both isoforms feature a polar heme-binding domain that is separated from a hydrophobic C-terminal membrane anchoring domain by a flexible medial region of approximately 20 residues (*1*). Most biophysical studies with b_5's are performed with variants comprising only the heme-binding domain due to their greater water solubility. The heme binding domains of Mc and OM b_5's are highly similar (*4*), consisting of two hydrophobic cores separated by a five-stranded β-sheet as originally demonstrated for bovine Mc b_5 (*5*) (see Figure 1). The order of secondary structural units in Mc and OM b_5 heme-binding domains is $\beta1-\alpha1-\beta4-\beta3-\mathbf{\alpha2-\alpha3-\beta5-\alpha4-\alpha5}-\beta2-\alpha6$. The units highlighted in bold form a four-helix bundle that defines the heme-binding pocket (core 1). For the purposes of the present work, we consider the remaining units of secondary structure to comprise core 2. Figure S1 (Supporting Information) provides amino acid sequence alignments for all known Mc and OM b_5 pairs from mammals. For consistency, in all cases we use the numbering scheme originally introduced by Mathews for the lipase fragment of bovine Mc b_5 (*6*).

One of the most intriguing differences between mammalian OM and Mc b_5's is that the former are considerably more stable toward denaturation (*7*, *8*). In striking contrast, we have found that bMc and rOM apocytochrome b_5 (apo-b_5) exhibit similar stability (*7*−*9*). While greater holoprotein stability may not by itself represent a functional advantage for mammalian OM b_5's relative to their Mc counterparts, we believe that a detailed understanding of its structural sources is important for the following reasons. First, it may be associated (*7*, *9*, *10*) with two other notable divergences in OM and Mc b_5 biophysical properties: (1) OM b_5 reduction potentials are more negative than those of Mc b_5's (*7*, *11*, *12*), suggesting a requirement for a greater electron delivery driving force; and (2) OM b_5's exhibit less extensive polypeptide dynamic mobility than do Mc b_5's (*13*−*15*), possibly reflecting greater specificity in interactions with

[†] This work was supported by a grant from the National Science Foundation (MCB-0446326).

[‡] PDB code for the R15H/A18S/E20S/I25L/I32L/L47R/L71S mutant of rat OM b_5: 2I89.

* To whom correspondence should be addressed. Phone: (785) 864-4090. Fax: (785)-864-5396. E-mail: drb@ku.edu.

[§] University of Kansas.

[#] Oklahoma Medical Research Foundation.

[1] Abbreviations: rOM b_5, rat outer mitochondrial membrane cytochrome b_5; bMc b_5, bovine microsomal cytochrome b_5; rMc b_5, rat microsomal cytochrome b_5; apo-b_5, apocytochrome b_5; CD, circular dichroism; DSC, differential scanning calorimetry.

10.1021/bi0615689 CCC: $33.50
Published on Web 10/26/2006

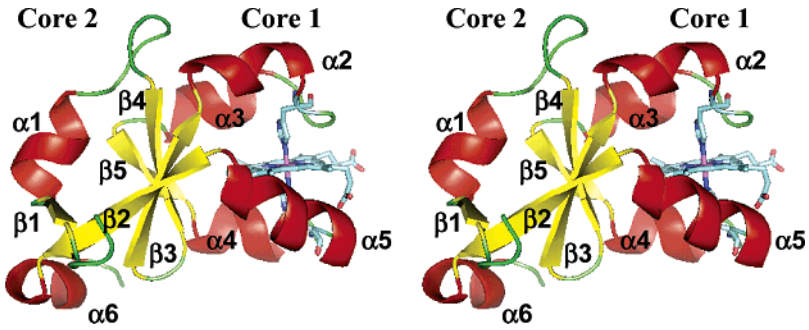

FIGURE 1: Stereoview of the crystal structure of bMc b_5 (PDB 1CYO) (*5*), highlighting the elements of secondary structure common to both Mc and OM b_5's and the relative locations of cores 1 and 2. The image was generated using PyMol v. 0.99 (*48*).

redox partners. Second, considered in the context of studies performed with b_5's from lower animals (*16*, *17*), it can shed light on the evolutionary history of Mc and OM b_5's. Third, it can guide the rational design of mutant b_5's having novel properties (*18*).

The divergent stability properties of OM and Mc b_5's appear to have arisen via the evolution of distinctly different packing motifs involving residues scattered throughout the protein sequences. For example, all OM b_5's contain an extended hydrophobic patch at the base of the heme binding pocket in core 1, involving the side chains of residues in and near the five-stranded β-sheet (*7*, *19*). Replacement of two distinct clusters in this hydrophobic patch in rat OM b_5 (rOM b_5) with the corresponding bovine Mc b_5 (bMc b_5) packing (*14*, *20*) yielded the rOM b_5 A18S/I25L/I32L/L47R/L71S quintuple mutant (hereafter OM^{5M} b_5), which exhibits a thermal denaturation midpoint more similar to that of bMc b_5 than of rOM b_5 (*20*). The decrease in holoprotein thermal stability that accompanied hydrophobic patch replacement was found to result from a >2 kcal/mol destabilization of rOM apo-b_5, however (*9*, *20*). More recently, we have shown that the hydrophobic patch replacement also disrupted rOM apo-b_5 core 2 conformation, as evidenced most notably by loss of a near-UV circular dichroism (CD) signal attributable to the side chain of Trp-22 (*19*).

Trp-22, invariant among known Mc and OM b_5's, is located in strand 4 of the β-sheet (β4). NMR studies of rat Mc (rMc) apo-b_5 by Moore and Lecomte (*21*, *22*) revealed that Trp-22 is part of an independent core 2 structural unit that also involves the side chains of two Tyr residues (Tyr-7 in β1 and Tyr-30 in β3), as well as Ile-75 and Ile-76 in β2, Val-29 in β3, and His-15 in a surface-exposed loop separating α1 and β4. The arrangement of the side chains of these residues, which are invariant among known mammalian Mc b_5's (Figure S1, Supporting Information), was found (*21*, *22*) to be virtually identical to that of the analogous residues in the X-ray crystal structure (*5*, *6*) of bMc b_5. A subset of the residues involved in this independent folding unit is shown in Figure 2A. Extension of these studies led to the discovery that nearly all of core 2 in rMc apo-b_5 is stably folded, whereas core 1 is almost completely disordered (*23*, *24*). Recent studies in our group indicate that the same is true of rOM apo-b_5 (*9*). In this context, it is worth noting that five of the seven invariant residues contributing to the independent mammalian Mc b_5 folding unit described above are also invariant among known mammalian OM b_5's: Trp-22, Tyr-7, Tyr-30, Ile-76, and Val-29. Mammalian OM b_5's differ from their Mc counterparts in this region at positions 15 (Arg rather than His) and 75 (Tyr rather than Ile). The difference at position 15 is highlighted in the rOM b_5 crystal structure [PDB 1B5M (*4*)] in Figure 2B.

The changes in stability and structural properties of rOM apo-b_5 caused by the hydrophobic cluster exchange described above were found to result almost entirely from a single point mutation: replacement of Leu-71, an invariant OM b_5 residue in core 1, with Ser, the corresponding invariant residue in mammalian Mc b_5's (*9*, *19*). These findings clearly showed that the similar stabilities exhibited by rOM and bMc apo-b_5 arise via distinctly different sets of conserved packing interactions. Specifically, we surmised that mammalian Mc b_5's harbor one or more conserved packing motifs that stabilize core 2 relative to the corresponding motifs in the OM isoform, thereby compensating for the presence of Ser at position 71 (*9*, *19*, *20*). Further supporting this hypothesis was the observation that bMc apo-b_5 retains considerably more secondary structure in the urea-denatured state than does urea-denatured rOM apo-b_5 (*9*). Herein we provide evidence that the greater core 2 stability exhibited by mammalian Mc apo-b_5's relative to their OM counterparts in both the folded and the unfolded states is due, in large measure, to the presence of His rather than Arg at position 15.

EXPERIMENTAL PROCEDURES

Site-Directed Mutagenesis. The recombinant pET11a-based plasmids harboring the genes coding for OM^{5M} b_5 (*20*) and bMc b_5 (*20*, *25*) were used to generate the genes for OM^{7M} b_5 and bMc H15R/S20E b_5, respectively, via the polymerase chain reaction (PCR). The primers designed for generating OM^{7M} b_5 were 5′-GAAGTTGCGAAACATAACACCTCTGAATCAACCTGG ATGGTTC-3′ and 5′-GAACCATCCAGGTTGATTCAGAGGTGTTATGTTTCGCAACTTC-3′. The corresponding primers designed for generating the H15R/S20E double mutant of bMc b_5 were 5′-GAAATCCAAAAACGCAACAACTCGAAAGAGACGTGGCTGA-3′ and 5′-TCAGCC ACGTCTCTTTCGAGTTGTTGCGTTTTTGGATTTC-3′. Underlined codons in each primer represent mismatches introduced to generate the mutations. The recombinant constructs were transformed into *Escherichia coli* DH5α competent cells for amplification. Once the mutations had been confirmed by sequencing, the recombinant plasmids carrying the mutant genes were transformed into *E. coli* BL21(DE3) cells for protein expression.

Protein Expression, Purification, and Characterization. Expression of the mutant proteins and subsequent steps

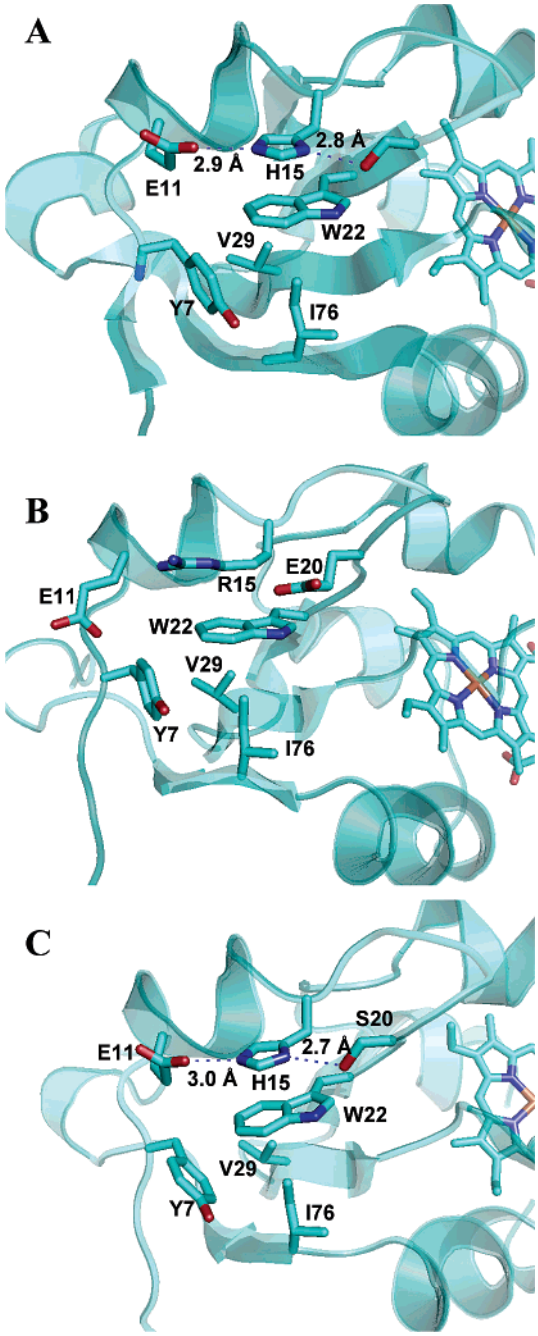

FIGURE 2: Packing in the vicinity of Trp-22 in bMc b_5 (A), rOM b_5 (B) and one of the four molecules in the unit cell of OM^{7M} b_5 (C). The images were generated using PyMol v. 0.99 (*48*). Additional information regarding the interactions between Glu-11, His-15, and Ser-20 is included in Table S2 (Supporting Information).

preceding their purification were accomplished using the published protocol for rOM b_5 (*26*) with the following modifications: (1) The expressions were performed at 27 °C rather than 37 °C with appropriate increases in incubation time both prior to and after induction with IPTG. This was done because recent studies have shown that the lower temperature enhances holoprotein yields, especially in cases where the apoprotein is thermally unstable (*9*). (2) A 0.1 M solution of hemin chloride in DMSO was added to the crude protein solution until UV/vis spectra indicated that no residual apoprotein remained (*23*). The sample was then passed through a disposable G-50 size exclusion column (Amersham) to remove excess hemin. The proteins were subsequently purified to homogeneity using a method recently developed for house fly cytochrome b_5 (*16*). Protein purity was assessed by native-PAGE, which allows us to detect the presence of residual apoprotein (*9*). The proteins were analyzed by electrospray ionization mass spectrometry (EI-MS) in the KU mass spectrometry laboratory, using conditions that caused essentially complete dissociation of hemin. The experimental mass closely matched the calculated mass of the polypeptide components of the two mutants. OM^{7M} b_5: 10 481 Da (experimental); 10 481 Da (calculated averaged MW). $bMc^{H15R/S20E}$ b_5: 9520.4 Da (experimental); 9522.48 (calculated averaged MW).

Table 1: Crystallography Data Collection and Refinement Statistics

Data Statistics	
space group	$P2_12_12_1$
unit cell (Å)	$a = 39.965$, $b = 51.409$, $c = 167.435$
mol in asymmetric unit cell	4
resolution (Å)	43.8−2.1 Å (2.18−2.1)[a]
R_{merge}	0.099 (0.48)[a]
no. of reflections	19485 (1844)[a]
completeness (%)	92.6 (90.4)[a]
I/σ	10.96 (2.6)[a]
redundancy	3.6
Refinement Statistics	
resolution (Å)	43.8−2.1
R_{work}	20.78 (for 16 823 reflections)
R_{free}	27.79 (for 1237 reflections)
no. of non hydr atoms	
protein (including heme)	2967
solvent	219
Mg ions	3
rms deviation from ideal values	
bond length (Å)	0.013
bond angle (°)	1.36
average B-factor	
protein	29.42
solvent	35.24
from Wilson plot	29.98

[a] Numbers in parentheses correspond to highest resolution shell.

Crystallization of OM^{7M} b_5. A batch of freshly expressed OM^{7M} b_5 was purified to homogeneity and concentrated to ~20 mg/mL in 20 mM Tris-HCl (pH 7.2). Crystallization was achieved at 5 °C using the hanging drop vapor diffusion method, from a solution containing 2 μL of stock solution described above mixed with an equal volume of reservoir solution containing 30% (w/v) polyethylene glycol 8000 (PEG8K), 0.1 M magnesium acetate, and 0.1 M PIPES at pH 6.8. The above solution was equilibrated against 500 mL of the reservoir solution. The first crystals appeared in 3 months, after the drops were seeded with microcrystals of house fly cytochrome b_5 (*16*). Prior to X-ray data collection at 100 K, a crystal of 0.1 × 0.1 × 0.02 mm was transferred to a cryosolution differing from the reservoir solution only by a higher concentration of PEG8K (36% w/v) and was flash cooled in a stream of nitrogen gas. A 93% complete data set was collected from a MAR345 image plate (Mar Research Inc., Norderstedt, Germany) installed on a Rigaku RU-H3R rotating anode X-ray generator (The Woodlands, TX) equipped with an Osmic Blue optics mirror system (Osmic Inc., Troy, MI) and Cryojet cooling system (Oxford instruments, Oxon, England). The images were processed with the program suite HKL (*27*). Some data collection statistics are included in Table 1.

Structure Solution and Refinement. The crystal, with unit cell parameters $a = 39.965$ Å, $b = 51.409$ Å, and $c = 167.435$ Å, belongs to the space group $P2_12_12_1$. The asymmetric unit cell contains four molecules of OM^{7M} b_5 and has a solvent content of 34%. This crystal form was isomorphous to the previously determined structure of the OM b_5 A18S/I32L/L47R triple mutant (PDB 1ICC) (*14*). We therefore replaced residues in that structure that have been mutated in OM^{7M} b_5 (Arg-15, Glu-20, Ile-25, and Leu-71) with alanines and used the resulting structure as a starting model in refinement carried out using the program suite CNS (*28*). After a cycle of simulated annealing (slow cooling protocol starting from 5000 K), the $2F_o - F_c$ and $F_o - F_c$ difference Fourier maps clearly showed additional densities for the residues occupying positions 15, 20, 25, and 71. The graphic program FRODO (*29*) was used to incorporate the actual residues occupying these positions into the structure. Three magnesium ions and 210 solvent molecules were gradually added to the refined model after a second cycle of simulated annealing, and this was followed by three cycles of positional and individual B-factor refinements. Bulk solvent and anisotropic overall B-factor corrections were applied throughout the refinement. The four heme groups were modeled and refined in the two orientational isomer forms, which differ by a 180° rotation about the porphyrin $\alpha-\gamma$-meso axis. In addition, Glu-11 in one of the molecules was refined with two different side chain conformations. In the final model, with $R_{work} = 0.21$ and $R_{free} = 0.28$ (calculated with a randomly selected 7% of the total reflections), all residues are within the most favored and additionally allowed regions of the Ramachandran plot as defined by program PROCHECK (*30*). Statistics on the refinement of OM^{7M} b_5 are summarized in the second part of Table 1. The atomic coordinates (PDB 2I89) have been deposited in the Protein Data Bank (*31*).

Apoprotein Preparation. Removal of hemin from the holoproteins was accomplished using the acid-butanone method of Teale (*32*). All apoproteins were used within 72 h of preparation. Apoprotein concentrations were determined from the absorbance at 280 nm, using an extinction coefficient calculated via an empirical equation (*33*) based on the number of Trp and Tyr residues in the protein ($\epsilon_{280} =$ 12 950 M^{-1} cm^{-1} for OM^{7M} apo-b_5; 11 260 $M^{-1}cm^{-1}$ for $bMc^{H15R/S20E}$ apo-b_5).

Thermal Denaturation of Holoproteins. Thermal denaturation experiments were performed on a Varian Carey 100 Bio UV/vis spectrophotometer, equipped with a Peltier-thermostated multiple cell holder and a dedicated temperature probe accessory (±0.1 °C). Solutions were buffered to pH 7.0 using 50 mM sodium phosphate. Protein concentrations ranged from 3 to 5 μM and were estimated using the absorbance at 412 nm (Soret band λ_{max}) and an extinction coefficient of 130 000 M^{-1} cm^{-1} (*34*). The temperature was increased in increments of 2 °C, and samples were equilibrated for 5 min after reaching each desired temperature. Thermal denaturation midpoints (T_m values) were obtained by fitting plots of absorbance at 412 nm vs temperature to an equation describing a two-state equilibrium and which corrects for nonzero baselines in the native and denatured regions (*35*). The unfolding reactions were not fully reversible, however, and we therefore did not attempt to extrapolate the data to obtain thermodynamic information.

Chemical Denaturation of Apoproteins. Urea-mediated denaturation experiments were performed at 25 °C, with solutions buffered to pH 7.0 using 30 mM MOPS. Urea stock solution concentrations were verified from measurements of the solution refractive index. All samples were incubated at 25 °C for 1 h before spectra were recorded. Chemical denaturation was monitored by fluorescence spectroscopy using a PTI QuantaMaster luminescence spectrometer (protein concentrations 0.5−1 μM), following changes in emission (340 nm) of Trp-22 (excitation at 295 nm). Data were fit to an equation describing a two-state equilibrium (see text for details) using Kaleidagraph v. 3.5 (Synergy Software).

Circular Dichroism Spectroscopy. Circular dichroism spectra were recorded on a Jasco J-710 spectropolarimeter equipped with a Jasco PTC-4235 Peltier-thermostated cell holder. Spectra were acquired at 1.0-nm intervals with a response time of 4 s and a scan rate of 50 nm/min and represent the average of at least five scans. Background correction was accomplished by subtraction of a spectrum recorded at the same temperature and containing only buffer.

Differential Scanning Calorimetry. Scanning calorimetry experiments with OM^{7M} apo-b_5 were performed on a Microcal VP-DSC microcalorimeter (Microcal Inc.) using a sample containing 1.83 mg/mL of apoprotein that had been extensively dialyzed (four changes of buffer every 6 h) against 50 mM potassium phosphate, pH 7.0. Immediately prior to each experiment, insolubles were removed by centrifugation at 12000*g* for 5 min, and the sample was degassed at 0.5 atm for 15 min. Prior to making measurements, baselines were established via repeated scans in which the sample cell contained buffer solution from the final dialysis step. Scans were performed from low to high temperatures ("upscans") at 1 K/min. Data were analyzed via a statistical mechanics-based deconvolution as implemented in the CSC 5100 software package to obtain the calorimetric enthalpy change (ΔH_{cal}).

RESULTS AND DISCUSSION

Identification of a Conserved Difference in Mc and OM b_5 Core 2 Packing. As noted in the introduction, mutating Leu-71 in rOM b_5 to Ser results in virtually complete disruption of well-defined tertiary structure in the vicinity of the Trp-22 side chain (*19*). This discovery prompted us to closely compare the Trp-22 side chain environment in the crystal structures of bMc b_5 (*5*) and rOM b_5 (*4*), in the context of amino acid sequences of all known Mc and OM b_5 pairs from mammals (see Figure S1, Supporting Information). In the bMc b_5 structure, we noted that the solvent-exposed, electron-poor side chain of His-15 is situated directly above the electron-rich six-membered ring of the Trp-22 side chain, in what appears to be an electron donor/acceptor π-stacking interaction (Figure 2A). In addition, the His-15 side chain in bMc b_5 forms hydrogen bonds with the side chains of Glu-11 and Ser-20, which like the contributors to the independent folding unit noted above are invariant among known mammalian Mc b_5's. In the rOM b_5 crystal structure (Figure 2B), the β, γ, and δ-CH_2 groups and the ϵ-NH group of solvent-exposed Arg-15 pack against the Trp-22 side chain. The Arg-15 ϵ-NH group also appears to engage in an electrostatic interaction with the Glu-20 carboxylate group (N−O distance 4.4 Å). The only known mammalian OM b_5

in which this packing motif differs is the bovine protein, in which residue 20 is Asp instead of Glu (Figure S1, Supporting Information).

We surmised that the His-15/Trp-22 π-stack and associated hydrogen-bonding interactions involving His-15 in mammalian Mc b_5's would provide greater stabilization to core 2 than would the corresponding packing motif in core 2 of the OM proteins. Hence, we considered it a likely factor contributing to the ability of core 2 in mammalian Mc apo-b_5's to adopt a stable fold despite the presence of Ser at position 71. Further supporting this hypothesis were literature reports showing that His−Trp interactions are statistically overrepresented in proteins (*36*) and that they can stabilize the native state (N) of a protein relative to the unfolded (U) state by up to 4 kcal/mol (*37*−*39*). The first step toward testing our prediction was to replace Arg-15 and Glu-20 in OM^{5M} b_5 with His and Ser, respectively, thereby generating the rOM b_5 R15H/A18S/E20S/I25L/I32L/L47R/L71S septuple mutant (hereafter OM^{7M} b_5).

X-ray Crystal Structure of OM^{7M} b_5. An X-ray crystal structure of OM^{7M} b_5 was obtained with a resolution of 2.1 Å. Data collection and refinement statistics are shown in Table 1. The diffraction data reveal four protein molecules per asymmetric unit cell. A π-stacking interaction between the His-15 and Trp-22 side chains is observed in all four molecules, and there is a hydrogen bond between the side chains of His-15 and Ser-20 as well. In two of the structures (Figure 2C), the Glu-11 side chain also forms a hydrogen bond with His-15, albeit with a different side chain conformation than that adopted by Glu-11 in bMc b_5. In a third molecule (not shown), the Glu-11 side chain is directed away from that of His-15 and toward the solvent, while in a fourth molecule (not shown) the Glu-11 side chain was resolved in two conformations, analogous to those observed in the two molecules just described. Notably, solution structures determined by NMR spectroscopy for rat Mc b_5 [PDB 1AW3 (*40*)] and rabbit Mc b_5 [PDB 1DO9 (*41*)] show the Ser-20 side chain hydrogen-bonded to that of His-15, and the Glu-11 side chain extending into solvent. Moreover, neither Glu-11 nor Ser-20 is hydrogen-bonded to His-15 in solution structures reported for two bMc b_5 length variants [PDB codes 1NX7 (*42*) and 1HXO (Muskett, F. W., and Whitford, D., unpublished results)]. We interpret these observations to indicate that the strength of interactions involving His-15 in OM^{7M} b_5 and Mc b_5's decrease in the order His-15/Trp-22 π-stack > His-15/Ser-20 H-bond > His-15/Glu-11 H-bond.

OM^{7M} b_5 Is More Thermostable than OM^{5M} b_5. Denaturation of cytochrome b_5 is accompanied by dissociation of the bonds between heme iron and axial ligands His-39 and His-63, converting Fe^{III} from the low-spin ($S = 1/2$) state to the high-spin ($S = 5/2$) state. The reactions can therefore be readily monitored by UV/vis spectroscopy. Because heme tends to aggregate extensively in aqueous solution (*43*), unfolding of holo-b_5 variants is only partially reversible. Hence, data obtained from such reactions cannot be extrapolated reliably through fits to equations based on equilibrium models. We have therefore generally opted to compare stabilities of holo-b_5 variants in terms of denaturation midpoints. Figure 3A compares a thermal denaturation curve for OM^{7M} b_5 with previously published curves for rOM b_5 and OM^{5M} b_5 (*20*). The curves, and the T_m values obtained from them (Table 2), show that OM^{7M} b_5 is markedly stabilized relative to OM^{5M} b_5.

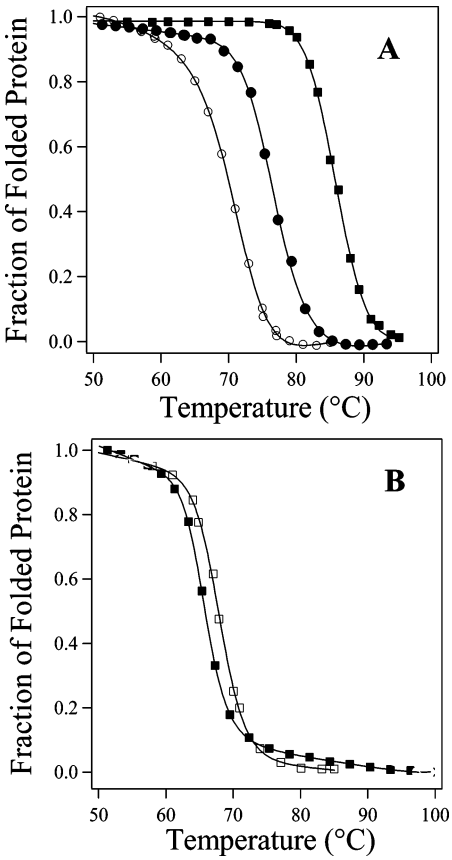

FIGURE 3: Thermal denaturation curves for (A) rOM b_5 (solid squares), OM^{5M} b_5 (open circles), and OM^{7M} b_5 (closed circles); and (B) bMc b_5 (open squares) and $bMc^{H15R/S20E}$ b_5 (solid squares).

Table 2: Data[a] from Holoprotein Thermal Denaturation[b] and Apoprotein Chemical Denaturation[c] Studies

	holoproteins	apoproteins		
b_5 variant	T_m (°C)	$\Delta G_{N\rightarrow U}$ (kcal/mol)	C_m (M urea)	M (kcal/mol/M)
rOM	85.5 ± 0.5	2.8 ± 0.1	2.5 ± 0.1	1.1 ± 0.1
OM^{5M}	69.0 ± 0.5	∼ −0.6	*d*	*d*
OM^{7M}	76.0 ± 0.5	*e*	*e*	*e*
bMc	67.6 ± 0.3	2.7 ± 0.1	4.1 ± 0.1	0.7 ± 0.1
$bMc^{H15R/S20E}$	64.2 ± 0.7	4.5 ± 0.3	∼2.5	1.8 ± 0.4

[a] Data for rOM, bMc and OM^{5M} b_5 are from ref 9. [b] Performed at pH 7.0 in 50 mM phosphate buffer. [c] Performed at 25 °C in 30 mM MOPS buffer. [d] Could not be determined. [e] Two-stage unfolding observed; see discussion in text.

The His-15/Trp-22 π-Stacking Interaction in OM^{7M} b_5 Appears To Persist in the Apoprotein. Urea-mediated denaturation of rOM and bMc apo-b_5 is conveniently probed by fluorescence spectroscopy, monitoring changes in fluorescence emission of Trp-22, which is the only tryptophan residue in each protein. In the course of such studies, we have discovered that Trp-22 fluorescence emission is much less intense in bMc apo-b_5 (Figure 4A; dashed line) than in rOM apo-b_5 (Figure 4A; solid line). Moreover, Trp-22 fluorescence intensity increases upon denaturation of bMc apo-b_5 (*44*, *45*) but decreases in the corresponding reaction of rOM apo-b_5. The decrease in Trp-22 fluorescence intensity that accompanies unfolding of rOM apo-b_5 can be explained by the fact that the Trp-22 side chain is moving from a well-

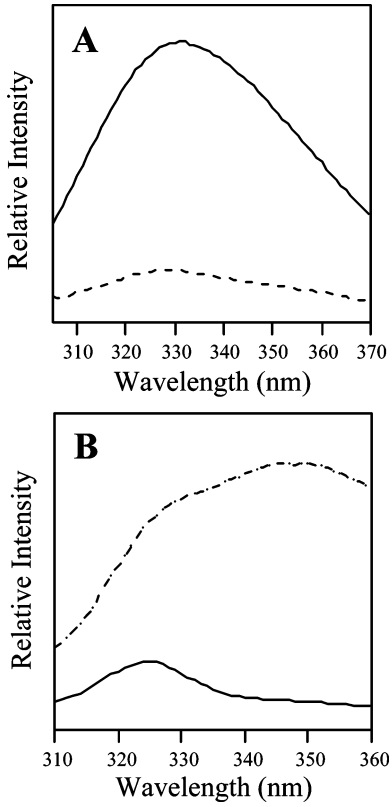

FIGURE 4: Fluorescence emission spectra. (A) rOM apo-b_5 (solid line) and bMc apo-b_5 (dashed line), each at 15 μM, and recorded sequentially using identical instrument settings. (B) OM^{7M} apo-b_5 in the native (solid line) and urea-denatured (dashed line) states. All data were recorded at 25 °C and pH 7.

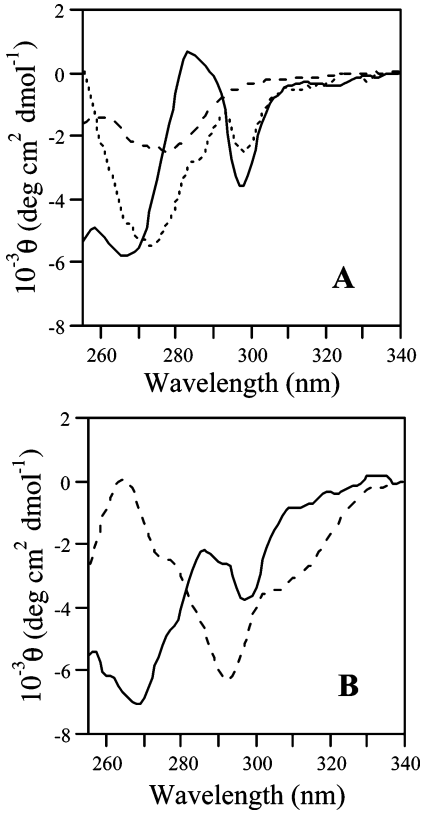

FIGURE 5: Near-UV CD data. (A) rOM apo-b_5 (solid line), OM^{5M} apo-b_5 (dashed line) and OM^{7M} apo-b_5 (dotted line). (B) bMc apo-b_5 (solid line) and $bMc^{H15R/S20E}$ apo-b_5 (dashed line). All spectra were recorded at 5 °C in 50 mM potassium phosphate, pH 7.0.

ordered environment in core 2 of the folded apoprotein to a less-ordered environment in the denatured state, thereby increasing the extent of nonradiative decay. Despite the disruption in Trp-22 environment in rOM apo-b_5 caused by the L71S mutation, urea-mediated denaturation of OM^{5M} apo-b_5 also results in diminished Trp-22 fluorescence intensity. While similar changes in Trp-22 fluorescence might be expected to occur upon bMc apo-b_5 unfolding, Trp-22 fluorescence emission in folded bMc apo-b_5 appears to be strongly quenched by the π-stacked side chain of His-15 (*44*). The increase in Trp-22 fluorescence emission resulting from disruption of the His-15/Trp-22 π-stack upon bMc apo-b_5 unfolding clearly outweighs the anticipated decrease resulting from its removal from a more-ordered to a less-ordered environment. Urea-mediated denaturation studies performed with OM^{7M} apo-b_5 reveal a nearly threefold increase in Trp-22 fluorescence emission intensity upon denaturation by urea (Figure 4B), rather than the decreases that are observed for rOM and OM^{5M} apo-b_5. This provides compelling evidence that the His-15/Trp-22 π-stacking interaction observed in the crystal structure of OM^{7M} b_5 remains intact following removal of heme from its binding pocket.

Converting OM^{5M} b_5 to OM^{7M} b_5 Largely Restores Apoprotein Core 2 Conformation. Side chains of aromatic amino acid residues in regions of well-defined tertiary structure exhibit CD signals in overlapping regions of the near-UV (Phe: 250−270 nm; Tyr: 270−290 nm; Trp: 280−300 nm) (*46*). As demonstrated initially by Huntley and Strittmatter (*44*), near-UV CD spectroscopy can provide useful information regarding structural integrity in core 2 of apo-b_5's. Figure 5A compares near-UV CD spectra of OM^{5M} and OM^{7M} apo-b_5 against a previously reported (*9*) spectrum of rOM apo-b_5. The near-UV CD spectrum of bMc apo-b_5 (*9*) appears in Figure 5B. All spectra in Figure 5A,B were recorded at 5 °C and pH 7 to maximize the amount of apoprotein present in the folded state. This is especially important in the case of OM^{5M} apo-b_5, which is only about 25% folded at 25 °C and pH 7 but is more than 90% folded at 5 °C and pH 7 (*9*). As previously reported, the near-UV CD spectra of rOM and bMc apo-b_5 are quite similar, with strong negative signals centered near 270 and 300 nm. The bands near 300 nm have been attributed to Trp-22 (*9*, *44*), which as already noted has its side chain in core 2. The signals near 270 nm likely arise primarily from the various Tyr residues, most of which also have their side chains in core 2. The near-UV CD spectrum of OM^{5M} apo-b_5 in Figure 5A is similar to the corresponding spectrum recently reported for rOM^{L71S} apo-b_5 (*19*) in that it lacks negative bands centered near 270 and 300 nm. Instead, it features a broad and relatively weak negative band centered near 278 nm. The changes in near-UV CD spectra that accompanied the conversion of rOM apo-b_5 to its L71S mutant served as our principal evidence that the mutation resulted in complete disruption of tertiary packing in the vicinity of Trp-22 and some Tyr residues in rOM apo-b_5. The presence of distinct signals in the near-UV CD spectrum of rOM^{L71S} apo-b_5 nonetheless suggested that core 2 still contained significant native-like tertiary structure, a conclusion that was supported by denaturation studies showing that OM^{L71S} apo-b_5 obeys a two-state unfolding equilibrium (*19*). It can likewise be concluded that the folded form of OM^{5M} apo-b_5 retains some hololike structure in core 2.

Figure 5A shows that converting OM^{5M} apo-b_5 to OM^{7M} apo-b_5 via the R15H/E20S double mutation is accompanied by reemergence of a negative band near 300 nm, indicating that the newly introduced packing motif rescues polypeptide conformational stability in the Trp-22 vicinity. The 300 nm band in the near-UV CD spectrum of OM^{7M} apo-b_5 is weaker than that in the spectrum of rOM apo-b_5, however. The near-UV CD spectrum of OM^{7M} apo-b_5 also exhibits enhanced intensity of the signal attributable to Tyr residues in core 2, although the position of that band is shifted relative to the corresponding band in the near-UV CD spectra of rOM and bMc apo-b_5. The results described in this section strongly suggest that incorporating the R15H/E20S double mutation into OM^{5M} apo-b_5 has largely restored holo-like tertiary structure to core 2, although differences clearly remain relative to both bMc and rOM apo-b_5.

OM^{7M} apo-b_5 Unfolds in Two Stages. Denaturation of rOM and bMc apo-b_5 by urea at pH 7 and 25 °C is reversible, and available evidence suggests that the reactions obey two-state equilibria (*9*). Figure 6A compares a urea-mediated denaturation curve for OM^{7M} apo-b_5, monitored by fluorescence spectroscopy, with previously published curves (*9*) for bMc, rOM, and OM^{5M} apo-b_5. The data are reported in terms of the fraction of protein that is folded at each urea concentration. The lines through the curves for bMc and rOM apo-b_5 in Figure 6A represent fits to an equation describing a two-state equilibrium (eq 1)

$$\text{fraction folded} = \{\exp[(\Delta G_{N\rightarrow U} - m[D])/RT]\}/\{1 + \exp[(\Delta G_{N\rightarrow U} - m[D])/RT]\} \quad (1)$$

$$\Delta G_{N\rightarrow U} = C_m m \quad (2)$$

where [*D*] is the concentration of urea, $\Delta G_{N\rightarrow U}$ is the free energy of unfolding in the absence of urea, and *m* is a parameter indicating the sensitivity of the free energy of unfolding to urea concentration. The concentration of urea at which each protein is 50% denatured (C_m value) was calculated using eq 2. $\Delta G_{N\rightarrow U}$, C_m and *m* values previously determined for bMc and rOM apo-b_5 using eqs 1 and 2 are included in Table 2. OM^{5M} apo-b_5 also appears to fold reversibly but is substantially unfolded at pH 7 and 25 °C (*9*, *20*). As a result, it was not possible to calculate $\Delta G_{N\rightarrow U}$, C_m, and *m* values for OM^{5M} apo-b_5 unfolding using eqs 1 and 2. On the basis of the apparent fraction of OM^{5M} apo-b_5 that is folded at pH 7 and 25 °C (~25%), however, we were able to conclude that it has a slightly negative unfolding free energy ($\Delta G_{N\rightarrow U} \sim -0.6$ kcal/mol; Table 2) (*9*, *20*).

As noted above, OM^{5M} apo-b_5 is only about 25% folded in the absence of urea at pH 7 and 25 °C (see Figure 6A). In contrast, the urea denaturation curve for OM^{7M} apo-b_5 in Figure 6A begins to level out at low urea concentrations, indicating that the protein is (1) predominantly folded in the absence of urea at pH 7 and 25 °C; and (2) more stable than OM^{5M} apo-b_5 under those conditions. The data in Figure 6A reveal an unfolding transition for OM^{7M} apo-b_5 that ends near [urea] = 2.8 M but is followed by a broad region exhibiting a gradual decrease in slope. We were intrigued by the fact that the initial region of the OM^{7M} apo-b_5 denaturation curve closely tracks that of rOM apo-b_5, while above [urea] = 5.8 M it closely tracks that of bMc apo-b_5. This led us to consider the possibility that OM^{7M} apo-b_5 denaturation proceeds in

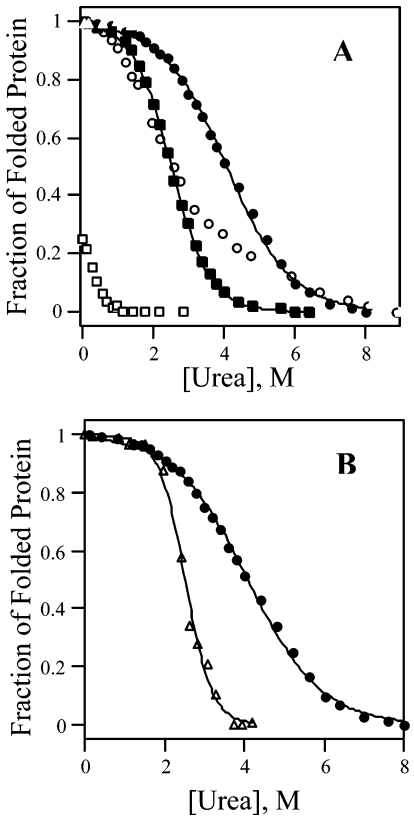

FIGURE 6: (A) Urea denaturation curves for OM^{7M} apo-b_5 (open circles), OM^{5M} apo-b_5 (open squares), rOM apo-b_5 (closed squares), and bMc apo-b_5 (closed circles). (B) Corresponding data for bMc apo-b_5 (closed circles) and $bMc^{H15R/S20E}$ apo-b_5 (open triangles). Lines through the curves represent fits of the data to an equation describing a two-state equilibrium (eq 1).

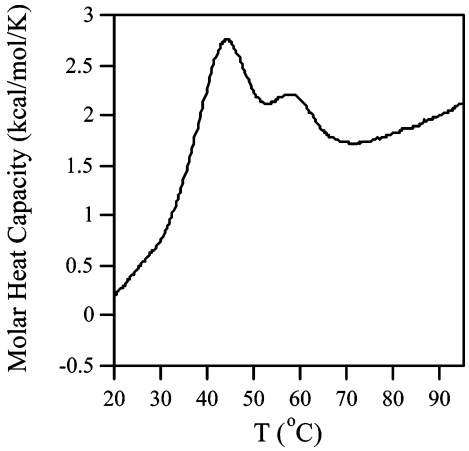

FIGURE 7: Differential scanning calorimetry data for OM^{7M} apo-b_5 (1.83 mg/mL), recorded in 50 mM potassium phosphate at pH 7.0.

two distinct stages, with the first stage involving C_m and *m* values similar to those exhibited by rOM apo-b_5 and the second stage involving C_m and *m* values similar to those displayed by bMc apo-b_5. To further probe this possibility, we pursued differential scanning calorimetry (DSC) experiments (Figure 7). The DSC data for OM^{7M} apo-b_5 in Figure 7 confirm that it unfolds in two distinct steps, in contrast to bMc, rOM, and rOM^{L71S} apo-b_5, which display single unfolding transitions (*9*,*19*). The lower temperature unfolding transition of OM^{7M} apo-b_5 has a midpoint value of $T_{m1} \sim 40$ °C, and an associated enthalpy change ($\Delta H_{cal,1}$) of ~26

kcal/mol. The higher temperature transition, with $T_{m2} = 58$ °C, involves an enthalpy increase of $\Delta H_{cal,2} \sim 12$ kcal/mol. A second upscan performed with the same sample of OM^{7M} apo-b_5 again indicated two unfolding transitions, but with less positive enthalpies and shifts in T_m values for both steps. This demonstrated that the unfolding reaction is not reversible, and we therefore made no attempt to fit the OM^{7M} apo-b_5 DSC data to a two-state model.

Confirmation of Our Hypothesis: The bMc b_5 H15R/S20E Double Mutant. The results of the preceding sections have demonstrated that introducing the R15H/E20S double mutation into OM^{5M} b_5 significantly stabilized the apoprotein and thereby the holoprotein. They also strongly suggest that the double mutation has substantially reversed the loss of structural integrity in core 2 that resulted from replacement of Leu-71 in core 1 with Ser. These results support, but do not prove, our hypothesis that the conserved His-15/Trp-22 π-stacking and Glu-11/His-15/Ser-20 hydrogen-bonding interactions in mammalian Mc b_5's help to counteract the destabilizing effect of having Ser at position 71. We therefore generated the H15R/S20E double mutant of bMc b_5 (hereafter $bMc^{H15R/S20E}$ b_5). The double mutation exerted a relatively small destabilizing effect on the holoprotein, with T_m decreasing from 67.6 to 64.2 °C (Figure 3B; Table 2), but its effects on bMc apo-b_5 properties were much more substantial. For example, the near-UV CD data in Figure 5B show that (1) the band of negative ellipticity near 270 nm in the spectrum of bMc apo-b_5 is replaced by a positive band in the corresponding spectrum of $bMc^{H15R/S20E}$ apo-b_5; and (2) the $bMc^{H15R/S20E}$ apo-b_5 spectrum contains a broad band centered near 292 nm with a shoulder at higher wavelength, rather than a relatively sharp band centered at 300 nm arising from Trp-22 as observed in bMc apo-b_5. These changes clearly indicate that core 2 structure in the vicinity of Trp-22 and at least some Tyr residues has been altered by the double mutation. The data suggest, however, that structure in the vicinity of Trp-22 is less disrupted by the H15R/S20E double mutation in bMc apo-b_5 than it was by the L71S mutation in rOM apo-b_5. This suggests the presence of additional packing interactions in Mc apo-b_5's that stabilize core 2 conformation in comparison to OM apo-b_5's. Future studies in our laboratories will be directed toward identifying those interactions.

Figure 6B shows that bMc and $bMc^{H15R/S20E}$ apo-b_5 also exhibit dramatically different urea-mediated unfolding curves. Urea-mediated denaturation curves obtained for $bMc^{H15R/S20E}$ apo-b_5 were of reproducibly poor quality, as reflected by the relatively high uncertainty of the $\Delta G_{N\rightarrow U}$ and m values in Table 2 obtained from fits of the data to eq 1. Nonetheless, the results of the fits suggest that the H15R/S20E double mutation has enhanced the stability of bMc apo-b_5, even though it led to a large decrease in C_m value. This apparent discrepancy can be explained by the fact that the mutation also led to a large increase in the slope of the unfolding transition, and thus a larger m value (see eq 2). A compelling explanation for the effect of the H15R/S20E double mutation on m value emerged when we compared far-UV CD spectra of bMc and $bMc^{H15R/S20E}$ apo-b_5 in the urea-denatured state. Previously published far-UV CD data revealed that bMc apo-b_5 retains considerably more secondary structure in the urea-denatured state (Figure 8, solid line) than does urea-denatured rOM apo-b_5 (Figure 8, dotted line) (*9*). The dashed line in

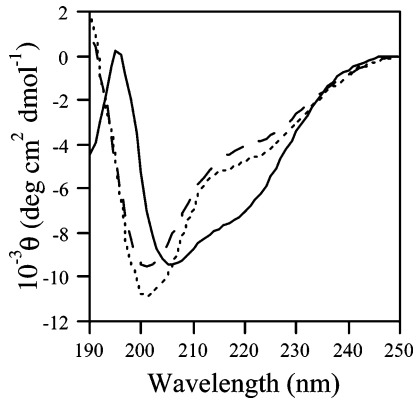

FIGURE 8: Far-UV CD spectra of urea-denatured bMc apo-b_5 (solid line), $bMc^{H15R/S20E}$ apo-b_5 (dashed line), and rOM apo-b_5 (dotted line). All spectra were recorded at 25 °C and pH 7.

Figure 8 shows that introducing the H15R/S20E double mutation into bMc apo-b_5 dramatically diminishes the extent of secondary structure in the unfolded state. In fact, the far-UV CD spectrum of urea-denatured $bMc^{H15R/S20E}$ apo-b_5 in Figure 8 is nearly identical to that of urea-denatured rOM apo-b_5. Hence, the R15H/S20E double mutation has likely increased the extent of bMc apo-b_5 polypeptide surface area that becomes exposed upon unfolding, a factor that is generally associated with increased m values (*47*). This striking observation strongly suggests that the extensive residual secondary structure in urea-denatured bMc apo-b_5 arises from the His-15/Trp-22 π-stacking interaction in core 2. It also implies that the second stage of OM^{7M} apo-b_5 heat- and urea-mediated unfolding involves disruption of the newly introduced His-15/Trp-22 π-stacking interaction.

The change in unfolded apoprotein structure revealed by far-UV CD spectroscopy may also help explain the apparent increase in bMc apo-b_5 thermodynamic stability resulting from the R15H/S20E double mutation: the double mutation may have destabilized the folded apoprotein as anticipated, but it may have destabilized the unfolded apoprotein to an even greater extent, thereby increasing $\Delta G_{N\rightarrow U}$.

Concluding Remarks. In previously reported studies, we have shown that replacing two conserved hydrophobic clusters in rOM b_5 with the corresponding Mc b_5 packing led to a substantial decrease in apoprotein stability (*9*, *20*). The hydrophobic cluster replacement also caused apoprotein conformational disorder to extend beyond the empty heme binding pocket and into core 2 (*19*). The point mutation found to be most responsible for these changes was replacement of Leu-71 in core 1 with Ser, which we found puzzling given that Leu-71 is located in disordered core 1. Our proposed explanation for the ability of Leu-71 to stabilize core 2 structure in rOM apo-b_5 (*19*) took into account the following considerations: (1) Leu-71 is located very close to the juncture between cores 1 and 2 (in the holoprotein, Leu-71 is in the final turn of helix α5); and (2) experimental data have indicated that rOM apo-b_5 has a much more compact empty heme-binding pocket than does bMc apo-b_5 (*9*, *19*). We surmised that the Leu-71 side chain would be able to engage in nonspecific hydrophobic interactions with apolar side chains of residues on the core 1 side of the β-sheet, including some that contribute to the extended hydrophobic patch in the holoprotein. Moreover, this hydrophobic cluster could attract hydrophobic side chains of

core 1 amino acids located more distant from the core 1/core 2 juncture, leading to a general "hydrophobic collapse" of the empty heme-binding pocket much more extensive than is possible in bMc apo-b_5. We proposed that the nonspecific interactions involving Leu-71 in core 1 and the associated hydrophobic collapse would provide stability to the β-sheet and, hence, to tertiary structure in core 2.

Available evidence indicates that core 2 structure in Mc apo-b_5's is independent of core 1. Indeed, it has been demonstrated that core 2 in rMc apo-b_5 folds even when core 1 has been excised from the protein (*35*). Herein we have provided evidence that this is due in large measure to the π-stacking interaction between the solvent-exposed side chain of His-15 and that of Trp-22, originally identified by NMR in the early 1990s as part of an independent folding unit in Mc apo-b_5 (*21*, *22*). We propose that this π-stacking interaction compensates for the absence of a hydrophobic residue at position 71 in core 1, aiding core 2 folding from within by substantially limiting Trp-22 side chain conformational mobility. In fact, the His-15/Trp-22 interaction in bMc apo-b_5 appears sufficiently strong to resist disruption even in 8 M urea, leading to an unusually large extent of secondary structure under those conditions.

ACKNOWLEDGMENT

We thank Prof. Russell Middaugh for use of his DSC equipment.

SUPPORTING INFORMATION AVAILABLE

Figure S1: comparison of amino acid sequences of the heme-binding domains of all known Mc and OM b_5 pairs from mammals; Table S1: information about the proteins included in Figure S1; Table S2: additional crystallographic data. This material is available free of charge via the Internet at http://pubs.acs.org.

REFERENCES

1. Lederer, F., Ghrir, R., Guiard, B., Cortial, S., and Ito, A. (1983) Two homologous cytochromes b_5 in a single cell, *Eur. J. Biochem. 132*, 95−102.
2. Guzov, V. M., Houston, H. L., Murataliev, M. B., Walker, F. A., and Feyereisen, R. (1996) Molecular cloning, overexpression in *Escherichia coli*, structural and functional characterization of house fly cytochrome b_5, *J. Biol. Chem. 271*, 26637−26645.
3. Kuroda, R., Ikenoue, T., Honsho, M., Tsujimoto, S., Mitoma, J., and Ito, A. (1998) Charged amino acids at the carboxy-terminal portions determine the intracellular locations of two isoforms of cytochrome b_5, *J. Biol. Chem. 273*, 31097−31102.
4. Rodriguez-Maranon, M. J., Qiu, F., Stark, R. E., White, S. P., Zhang, X., Foundling, S. I., Rodriguez, V., Schilling, I. I. I., C. L., Bunce, R. A., and Rivera, M. (1996) ^{13}C NMR spectroscopic and X-ray crystallographic study of the role played by mitochondrial cytochrome b_5 heme propionates in the electrostatic binding to cytochrome *c*, *Biochemistry 35*, 16378−16390.
5. Durley, R. C. E., and Mathews, F. S. (1996) Refinement and structural analysis of bovine cytochrome b_5 at 1.5 Å resolution, *Acta Crystallogr. D52*, 65-76.
6. Mathews, F. S., Gerwinsky, E. W., and Argos, P. (1979) The X-ray crystallographic structure of calf liver cytochrome b_5, in *The Porphyrins* (Dolphin, D., Ed.) pp 107−147, Academic Press, New York.
7. Altuve, A., Wang, L., Benson, D. R., and Rivera, M. (2004) Mammalian mitochondrial and microsomal cytochromes b_5 exhibit divergent structural and biophysical characteristics, *Biochem. Biophys. Res. Commun. 314*, 602−609.
8. Silchenko, S., Sippel, M. L., Kuchment, O., Benson, D. R., Mauk, A. G., Altuve, A., and Rivera, M. (2000) Hemin is kinetically trapped in cytochrome b_5 from rat outer mitochondrial membrane, *Biochem. Biophys. Res. Commun. 271*, 467−472.
9. Cowley, A. B., Rivera, M., and Benson, D. R. (2004) Stabilizing roles of residual structure in the empty heme binding pockets and unfolded states of microsomal and mitochondrial apocytochrome b_5, *Protein Sci. 13*, 2316−2329.
10. Cowley, A. B., Kennedy, M. L., Silchenko, S., Lukat-Rodgers, G. S., Rodgers, K. R., and Benson, D. R. (2006) Insight into heme protein redox potential control and functional aspects of six-coordinate ligand-sensing heme proteins from studies of synthetic heme peptides, *Inorg. Chem. 45*, in press.
11. Rivera, M., Seetharaman, R., Girdhar, D., Wirtz, M., Zhang, X., Wang, X., and White, S. (1998) The reduction potential of cytochrome b_5 is modified by its exposed heme edge, *Biochemistry 37*, 1485−1494.
12. Rivera, M., Wells, M. A., and Walker, F. A. (1994) Cation-promoted cyclic voltammetry of recombinant rat outer mitochondrial membrane cytochrome b_5 at a gold electrode modified with β-mercaptopropionic acid, *Biochemistry 33*, 2161−2170.
13. Simeonov, M., Altuve, A., Massiah, M. A., Wang, A., Eastman, M. A., Benson, D. R., and Rivera, M. (2005) Mitochondrial and microsomal ferric b_5 cytochromes exhibit divergent conformational plasticity in the context of a common fold, *Biochemistry 44*, 9308−9319.
14. Altuve, A., Silchenko, S., Lee, K. -. H., Kuczera, K., Terzyan, S., Zhang, X., Benson, D. R., and Rivera, M. (2001) Probing the differences between rat liver outer mitochondrial membrane cytochrome b_5 and microsomal cytochromes b_5, *Biochemistry 40*, 9469−9483.
15. Lee, K.-H., and Kuczera, K. (2003) Molecular dynamics simulation studies of cytochrome b_5 from outer mitochondrial and microsomal membrane, *Biopolymers. 69*, 260−269.
16. Wang, L., Cowley, A. B., Terzyan, S., Zhang, X., and Benson, D. R. (2006) Comparison of cytochromes b_5 from insects and vertebrates. *Proteins*, in press.
17. Wang, L., Urbauer, R. J. B., Urbauer, J. L., and Benson, D. R. (2003) House fly cytochrome b_5 exhibits kinetically trapped hemin and selectivity in hemin binding, *Biochem. Biophys. Res. Commun. 305*, 840−845.
18. Sun, N., Wang, A., Cowley, A. B., Altuve, A., Rivera, M., and Benson, D. R. (2005) Enhancing the stability of microsomal cytochrome b_5: a rational approach informed by comparative studies with the outer mitochondrial membrane isoform, *Protein Eng., Des., Select. 18*, 571−579.
19. Cowley, A. B., Sun, N., Rivera, M., and Benson, D. R. (2005) Divergence in non-specific hydrophobic packing interactions in the apo state, and its possible role in functional specialization of mitochondrial and microsomal cytochrome b_5, *Biochemistry 44*, 14606−14615.
20. Cowley, A. B., Altuve, A., Kuchment, O., Terzyan, S., Zhang, X., Rivera, M., and Benson, D. R. (2002) Toward engineering the stability and hemin binding properties of microsomal cytochromes b_5 into rat outer mitochondrial membrane cytochrome b_5: examining the influence of residues 25 and 71, *Biochemistry 41*, 11566−11581.
21. Moore, C. D., and Lecomte, J. T. J. (1990) Structural properties of apocytochrome b_5: Presence of a stable native core, *Biochemistry 29*, 1984−1989.
22. Moore, C. D., and Lecomte, J. T. J. (1993) Characterization of an independent structural unit in apocytochrome b_5, *Biochemistry 32*, 199−207.
23. Falzone, C. J., Mayer, M. R., Whiteman, E. L., Moore, C. D., and Lecomte, J. T. J. (1996) Design challenges for hemoproteins: The solution structure of apocytochrome b_5, *Biochemistry 35*, 6519−6526.
24. Falzone, C. J., Wang, Y., Vu, B. C., Scott, N. L., Bhattacharya, S., and Lecomte, J. T. J. (2001) Structural and dynamic perturbations induced by heme binding in cytochrome b_5, *Biochemistry 40*, 4879−4891.
25. Funk, W. D., Lo, T. P., Mauk, M. R., Brayer, G. D., MacGillivray, R. T. A., and Mauk, A. G. (1990) Mutagenic, electrochemical, and crystallographic investigation of the cytochrome b_5 oxidation-reduction equilibrium: Involvement of asparagine-57, serine-64, and heme propionate-7, *Biochemistry 29*, 5500−5508.
26. Rivera, M., Barillas-Mury, C., Christensen, K. A., Little, J. W., Wells, M. A., and Walker, F. A. (1992) Gene synthesis, bacterial expression, and ^{1}H NMR spectroscopic studies of the rat outer mitochondrial membrane cytochrome b_5, *Biochemistry 31*, 12233−12240.

27. Otwinowski, Z., and Minor, W. (1997) Processing of X-ray diffraction data collected in oscillation mode, *Methods Enzymol. 276*, 307−326.
28. Brunger, A. T., Adams, P. D., Clore, G. M., DeLano, W. L., Gros, P., Grosse-Kunstleve, R. W., Jiang, J. S., Kuszewski, J., Nilges, M., and Pannu, N. S. (1998) Crystallography and NMR system: A new software suite for macromolecular structure determination, *Acta Crystallogr. D54*, 905−921.
29. Roussel, A., and Cambillau, C. (1989) TURBO-FRODO, in *Silicon Graphics Geometry Partners Directory*, pp 77-79, Silicon Graphics, Mountain View, CA.
30. Laskowski, R. A., MacArthur, M. W., Moss, D. S., and Thornton, J. M. (1993) PROCHECK: a program to check the stereochemical quality of protein structures, *J. Appl. Crystallogr. 26*, 283−291.
31. Berman, H. M., Westbrook, J., Feng, Z., Gilliland, G., Bhat, T. N., Weissig, H., Shindyalov, I. N., and Bourne, P. E. (2000) The protein data bank. *Nucl. Acids Res. 28*, 235−242.
32. Teale, F. W. J. (1959) Cleavage of the haem-protein link by acid methylethylketone, *Biochim. Biophys. Acta. 35*, 453.
33. Gill, S. C., and von Hippel, P. H. (1989) Calculation of protein extinction coefficients from amino acid sequence data, *Anal. Biochem. 182*, 319−326.
34. Beck von Bodman, S., Schuler, M. A., Jollie, D. R., and Sligar, S. G. (1986) Synthesis, bacterial expression, and mutagenesis of the gene coding for mammalian cytochrome b_5, *Proc. Natl. Acad. Sci. U.S.A. 83*, 9443−9447.
35. Constans, A. J., Mayer, M. R., Sukits, S. F., and Lecomte, J. T. J. (1998) A test of the relationship between sequence and structure in proteins: Excision of the heme binding site in apocytochrome b_5, *Protein Sci. 7*, 1983−1993.
36. Samanta, U., and Chakrabarti, D. P. P. (2000) Environment of tryptophan side chains in proteins, *Proteins. 38*, 288−300.
37. Loewenthal, R., Sancho, J., and Fersht, A. R. (1991) Fluorescence spectrum of barnase: Contributions of three tryptophan residues and a histidine-related pH dependence, *Biochemistry 30*, 6775−6779.
38. Matthews, J. M., Ward, L. D., Hammacher, A., Norton, R. S., and Simpson, R. J. (1997) Roles of histidine 31 and tryptophan 34 in the structure, self-association, and folding of murine interleukin-6, *Biochemistry 36*, 6187−6196.
39. Dalhus, B., Saarinen, M., Sauer, U. H., Eklund, P., Johansson, K., Karlsson, A., Ramaswamy, S., Bjork, A., Synstad, B., and Naterstad, K. (2002) Structural basis for thermophilic protein stability: Structures of thermophilic and mesophilic malate dehydrogenases, *J. Mol. Biol. 318*, 707−721.
40. Arnesano, F., Banci, L., Bertini, I., and Felli, I. C. (1998) The solution structure of oxidized rat microsomal cytochrome b_5, *Biochemistry 37*, 173−184.
41. Banci, L., Bertini, I., Rosato, A., and Scacchieri, S. (2000) Solution structure of oxidized microsomal rabbit cytochrome b_5, *Eur. J. Biochem. 267*, 755−766.
42. Zhang, Q., Cao, C., Wang, Z. -. Q., Wang, Y. -. H., Wu, H., and Huang, Z.-X. (2004) The comparative study on the solution structures of the oxidized bovine microsomal cytochrome b_5 and mutant V45H, *Protein Sci. 13*, 2161−2169.
43. White, W. I. (1978) Aggregation of porphyrins and metalloporphyrins, in *The Porphyrins* (Dolphin, D., Ed.) Chapter 7, Academic Press, New York.
44. Huntley, T. E., and Strittmatter, P. (1972) The effect of heme binding on the tryptophan residue and the protein conformation of cytochrome b_5, *J. Biol. Chem. 247*, 4641−4647.
45. Manyusa, S., and Whitford, D. (1999) Defining folding and unfolding reactions of apocytochrome b_5 using equilibrium and kinetic fluorescence measurements, *Biochemistry 38*, 9533−9540.
46. Kahn, P. C. (1979) The interpretation of near-ultraviolet circular dichroism, *Methods Enzymol. 61*, 339−378.
47. Myers, J. K., Pace, C. N., and Scholtz, J. M. (1995) Denaturant *m* values and heat capacity changes: Relation to changes in accessible surface areas of protein unfolding, *Protein Sci. 4*, 2138−2148.
48. DeLano, W. L. (2002) DeLano Scientific, San Carlos, CA.

BI0615689